Daily Oscillation of the Excitation/Inhibition Ratio is Disrupted in Two Mouse Models of Autism

Michelle C.D. Bridi[1], Nancy Luo[1], Grace Kim[1], Caroline O'Ferrall[2], Ruchit Patel[2], Sarah Bertrand[2], Sujatha Kannan[2], and Alfredo Kirkwood[1]

[1]Zanvyl Krieger Mind/Brain Institute, Johns Hopkins University, Baltimore, MD

[2]Department of Anesthesiology and Critical Care Medicine, Johns Hopkins University School of Medicine, Baltimore, MD

ABSTRACT

Autism spectrum disorder (ASD) is a prevalent neurodevelopmental disorder involving sensory processing abnormalities. Alterations to the balance between excitation and inhibition (E/I ratio) are postulated to underlie behavioral phenotypes in ASD patients and mouse models. However, in primary visual cortex (V1) of wild type mice, the E/I ratio is not a fixed value, but rather oscillates across the 24h day. Therefore, we hypothesized that the E/I oscillation, rather than the overall E/I ratio, may be disrupted in ASD mouse models. To this end, we measured the E/I ratio in *Fmr1* KO and BTBR mice, models of syndromic and idiopathic ASD, respectively. We found that the E/I ratio is dysregulated in both models, but in different ways: the oscillation is flattened in *Fmr1* KO and phase-shifted in BTBR mice. These phenotypes cannot be explained by altered sleep timing, which was largely normal in both lines. Furthermore, we found that E/I dysregulation occurs due to alterations in both excitatory and inhibitory synaptic transmission in both models. These findings provide a crucial perspective on the E/I ratio in ASD, suggesting that ASD phenotypes may be produced by a mismatch of E/I to the appropriate behavioral state, rather than alterations to overall E/I levels *per se*.

INTRODUCTION

Autism spectrum disorder (ASD) is a prevalent neurodevelopmental disorder estimated to affect 1 in 54 children (Maenner et al., 2020). The core features of ASD are language deficits, social interaction deficits, and repetitive or restrictive behaviors and interests. These features are accompanied by sensory abnormalities in >90% of cases, and sensory processing differences have been reported to affect every sensory modality (reviewed in Geschwind, 2009; Robertson and Baron-Cohen, 2017). Visual processing in particular is of great interest, as behavioral deficits have been tied to altered processing in the primary visual cortex (V1) of *Fmr1* knockout (KO) mice (Goel et al., 2018). Therefore, investigating how sensory processing is altered is crucial to our understanding of ASD.

ASD is genetically diverse, but elevation of the ratio between excitatory and inhibitory signaling (E/I ratio) in the brain has been proposed as a unifying mechanism (Rubenstein and Merzenich, 2003). Accordingly, higher E/I ratio and/or lower inhibition has been observed in sensory cortices of many ASD mouse models (Antoine et al., 2019; Banerjee et al., 2016; Bridi et al., 2017; Cellot and Cherubini, 2014; Chao et al., 2010; Gibson et al., 2008; Wallace et al., 2012; Zhang et al., 2014; Zhao and Yoshii, 2019). However, the opposite (decreased E/I ratio, increased inhibition, and/or decreased excitation) has also been reported (Dani et al., 2005; Delattre et al., 2013; Etherton et al., 2011; Harrington et al., 2016; Tabuchi et al., 2007; Unichenko et al., 2018).

One possible explanation for these opposing findings is that regulation of the E/I ratio, rather than the E/I ratio itself, is disrupted in ASD. In wild type (WT) mice, the E/I ratio in primary visual cortex (V1) changes over the course of the 24h light:dark cycle, such that it is higher when animals have been in the dark (active) phase than when they have been in the light (rest) phase (Bridi et al., 2020). Therefore, an apparent elevation of the E/I ratio in ASD models could be due to increased E/I at all times of day, or due to dysregulation (flattening or phase shift) of the E/I oscillation. In the latter case, whether the E/I ratio appears higher or lower in ASD models would depend on time of day it is measured. However, prior studies have generally sampled a single time point, making it impossible to distinguish between these possibilities.

These considerations prompted us to examine possible E/I ratio dysregulation in two ASD mouse models with disparate genetic causes: the *Fmr1* knockout (*Fmr1* KO) mouse, which models Fragile X syndrome (Bakker et al., 1994), the most frequent monogenic cause of intellectual disability and ASD in humans (Hagerman et al., 2017), and the BTBR *T+ Itpr3*^{tf}*/J* (BTBR) mouse, an inbred line that models idiopathic ASD (McFarlane et al., 2008; Meyza and Blanchard, 2017). We show that the E/I ratio is dysregulated in both *Fmr1* KO and BTBR mice but in different ways: the oscillation is flattened in *Fmr1* KO mice and phase-shifted in BTBR mice. We found only minor differences in sleep architecture and quality, suggesting that disturbed sleep is not responsible for the E/I dysregulation observed in these models. Furthermore, we found that dysregulated E/I ratio oscillations are caused by alterations to both excitatory and inhibitory synaptic transmission. Therefore, exploration of the mechanisms that control these processes will provide further insight into the pathophysiology of ASD in the future.

METHODS

Animals

All procedures were approved by the Johns Hopkins University Institutional Animal Care and Use Committee. Mice were bred in-house on a 12:12 light:dark cycle (lights on at 7AM). Upon weaning, naïve mice were entrained for at least two weeks to a 12:12 light:dark cycle in custom entrainment chambers, with the timing of lights-on adjusted according to the experiment. Due to X-linkage of the *Fmr1* gene, only male *Fmr1* WT and KO mice were used. C57Bl/6J and BTBR mice of either sex were used. Littermates were distributed across experimental groups.

Slice Preparation

300 μm thick coronal brain slices containing V1 were prepared as described previously (Bridi et al., 2020). Briefly, slices were cut in ice-cold dissection buffer containing 212.7 mM sucrose, 5 mM KCl, 1.25 mM NaH_2PO_4, 10 mM $MgCl_2$, 0.5 mM $CaCl_2$, 26 mM $NaHCO_3$, and 10 mM dextrose, bubbled with 95% O_2/5% CO_2 (pH 7.4). Slices were transferred to normal artificial cerebrospinal fluid (similar to the dissection buffer except that sucrose was replaced by 119 mM NaCl, $MgCl_2$ was lowered to 1 mM, and $CaCl_2$ was raised to 2 mM) and incubated at 30 ˚C for 30 min and then at room temperature for at least 30 min before recording.

Whole-Cell Recording

Visualized whole-cell voltage clamp recordings were made from pyramidal neurons in L2/3 (35% depth from the pia) of V1. Glass pipette recording electrodes (3–6 MΩ) were filled with different internal solutions according to each experiment, all of which were adjusted to pH 7.2–7.3, 280–295 mOsm. Cells with an input resistance ≥ 150 MΩ and access resistance ≤ 25 MΩ were recorded. For all whole cell recordings, cells were discarded if these values changed more than 25% during the experiment. Data were filtered at 2 kHz and digitized at 10 kHz using Igor Pro (WaveMetrics, Portland, OR).

E/I ratio. The internal pipette solution for recording evoked EPSCs and IPSCs contained 8mM KCl, 125 mM cesium gluconate, 10 mM HEPES, 1 mM EGTA, 4mM Mg-ATP, 0.5mM Na-GTP, and 5 mM QX-314-Br. Responses were recorded in the presence of 100 μM DL-APV . Reversal potentials for excitatory and inhibitory currents of +10 mV and -55 mV (without junction potential compensation) were used (Bridi et al., 2020). To evoke synaptic responses, a double-barrel glass stimulating pipette filled with ACSF was placed approximately 100 □m lateral to the recording electrode (layer 2/3 stimulation) or in the middle of the cortical thickness (layer 4 stimulation). A series of stimulations over a range of intensities was delivered, and the responses over the range of intensities producing a stable E/I ratio were used (Bridi et al., 2020).

E/I ratio quantification. Peak response amplitude at each holding potential was measured for each stimulus intensity and the ratio between the excitatory and inhibitory peak was calculated (Igor Pro). If multiple peaks were observed in the postsynaptic response, the magnitude of the first peak was used in order to limit the analysis to monosynaptic responses. If the first peak could not be clearly resolved, the cell was discarded from the analysis.

Miniature postsynaptic current recordings. For mEPSC recordings, 1 μM TTX, 100 μM DL-APV and 2.5 μM gabazine were added to the perfusion buffer to isolate AMPAR-mediated mEPSCs.

An internal pipette solution containing the following ingredients was used: 8 mM KCl, 125 mM cesium gluconate, 10 mM HEPES, 1 mM EGTA, 4 mM NaATP, and 5 mM QX-314-Br. To record mIPSCs, 1 μM TTX, 100 μM DL-APV and 20 μM CNQX were included in the bath. The internal pipette solution contained: 8 mM NaCl, 120 mM cesium chloride, 10 mM HEPES, 2 mM EGTA, 4 mM MgATP, 0.5 mM NaGTP, and 10 mM QX-314-Br. V_m was held at -70 mV.

mEPSCs and mIPSCs were detected and analyzed using the MiniAnalysis program (Synaptosoft, Decatur, GA). Only cells with root mean square (RMS) noise <2 (mEPSCs) or <4 (mIPSCs) were included in the analysis and event detection threshold was set at 3 times the RMS noise. 300 events with rise time <3 msec (mEPSCs) or <5 msec (mIPSCs) were selected for each cell to calculate frequency and amplitude. Non-overlapping events were used to construct the averaged traces.

Polysomnography recording

Surgery. 4-5 week old mice were placed under isoflurane (1-2%) anesthesia and immobilized. A pocket was formed under the skin and a wireless transponder attached to four recording leads (model HD-X02, Data Sciences International, St. Paul, MN) was inserted into the pocket. Two EMG leads with 0.5 cm exposed wire were inserted into the cervical trapezius muscles and held in place with 5-0 silk sutures. The skull was cleaned with H_2O_2 and two holes were drilled for EEG lead placement (location posterior to bregma/lateral to the midline: 3.4mm/2.5mm and 1mm/1mm). EEG leads with 1-2 mm exposed wire were inserted into the holes to make contact with the dura and affixed with dental acrylic and cyanoacrylate glue. The wound was sutured closed and treated with triple antibiotic ointment. Mice were allowed to recover in their home cage for at least 7 days before recording. Home cages were then placed on top of telemetry receiver pads and EEG and EMG signals were captured (Data Sciences International, PhysioTel Receiver RPC-1) using Ponemah software (Data Sciences International, Version 6.40) for 3 consecutive days on a light-dark cycle matching the vivarium environment. The EEG/EMG signal was sampled at 500 Hz.

Arousal stages were scored manually off-line as NREM sleep, REM sleep, and wake by a trained experimenter (MB) in 4-s epochs (SleepSign for Animal, Kissei Comtec). The percent time spent in each state, along with number and duration of bouts, was calculated. Power spectra were computed within each arousal state by performing a fast Fourier transform on the EEG signal with 0.5 Hz resolution. For each arousal state, spectra were normalized to the total EEG power (0.5-80 Hz) in that state. One B6 and one BTBR animal were included in sleep architecture analysis but excluded from spectral analysis due to differences in electrode placement.

Statistics

Data were analyzed with 2-tailed unpaired t-tests, Wilcoxon rank-sum tests, 2-way repeated measures ANOVAs with Holm-Sidak posthoc analysis, or Kruskal-Wallis with Dunn's posthoc analysis, as indicated in the figure legends (GraphPad Prism, San Diego, CA). $P < 0.05$ was considered significant. The in cases where data were not normally distributed (Kolmogorov-Smirnov normality test), nonparametric tests were used. Sample size is displayed in the figures as (number of cells, number of animals). Lines and error bars in all figure dot plots indicate mean and SEM.

RESULTS

The E/I ratio is dysregulated in two mouse models of ASD.

We first determined whether the E/I ratio is dysregulated across the 24-h light/dark cycle in *Fmr1* KO mice. We measured the E/I ratio by recording excitatory and inhibitory synaptic responses in pyramidal cells in V1 layer 2/3, in response to electrical stimulation lateral to the recording electrode (Fig. 1A). We first measured E/I at two time points: ZT0 and ZT12. As expected, in *Fmr1* WT controls, the E/I ratio was higher at ZT0 ($t_{(51)}$=3.92, P=0.0003, unpaired t test). In contrast, the E/I ratio in *Fmr1* KO animals was not different between ZT0 and ZT12 (U=312, P=0.22, Mann-Whitney U test). These findings are consistent with two scenarios: the daily oscillation in E/I ratio is either shifted in time or flattened in these animals. To distinguish these possibilities, we then included additional time points (ZT6, 18; Fig. 1A). While the E/I ratio in *Fmr1* WT animals was higher when the animal had been in the dark phase (ZT0, 18), it did not differ across time points for the *Fmr1* KO animals, indicating that the E/I oscillation is flattened (Fig. 1B).

We then examined the E/I ratio in BTBR and C57Bl/6J control mice at ZT0 and ZT12 (Fig. 1A). As expected, B6 controls exhibited a higher E/I ratio at ZT0 than at ZT12 (Fig. 1C). In contrast, the E/I ratio in the BTBR mice showed the opposite pattern, with a higher E/I ratio at ZT12 than ZT0 (Fig. 1C). This indicates that the E/I oscillation is not lost in BTBR mice, but is shifted in time. Therefore, the E/I oscillation in both ASD models is disrupted, but in different ways.

The E/I ratio oscillates over the 24h day in the lateral (layer 2/3-2/3) circuit, but not in the feedforward (layer 4-2/3) circuit in V1 of WT mice (Bridi et al., 2020). We wished to confirm that *Fmr1* KO and BTBR mice did not display an abnormal oscillation in this circuit. To this end, we electrically stimulated layer 4 while recording synaptic currents in layer 2/3 of V1 slices. We confirmed that the E/I ratio did not change across the day for *Fmr1* KO, *Fmr1* WT, BTBR, or B6 animals (Fig. S1). It has been reported in primary somatosensory cortex (S1) that *Fmr1* KO mice have an elevated E/I ratio in the layer 4-2/3 circuit (Antoine et al., 2019), so we also examined whether there was an overall E/I elevation in this circuit in V1. However, there was no main effect of genotype or a genotype × time interaction for either ASD model (Fig. S1).

Altered sleep timing does not explain E/I dysregulation in two mouse models of ASD.

Sleep is thought to regulate the oscillation of both excitatory and inhibitory synaptic transmission over the course of the day (Bridi et al., 2020; Liu et al., 2010). Therefore, it is possible that the observed E/I dysregulation in *Fmr1* KO and BTBR mice is due to abnormal sleep timing. Indeed, *Fmr1* KO mice have been reported to have decreased total sleep and decreased numbers of REM bouts during the light phase (Boone et al., 2018; Saré et al., 2017); however, no studies to date have performed round-the-clock polysomnographic recordings in *Fmr1* KO or BTBR mice. We investigated this possibility by continuously recording EEG and EMG signals in the home cage using wireless telemetry for three days. We found that sleep architecture and timing was grossly normal in *Fmr1* KO and BTBR mice compared to their respective controls (Fig. 2; Fig. S2A-D). Overall amounts of wake, non-REM (NREM) sleep, and REM sleep did not differ between *Fmr1* KO and WT or between BTBR and B6 mice (Fig. S2A). Furthermore, the distribution of time spent in each state across the day did not differ between *Fmr1* KO and WT mice (Fig. 2A). The overall pattern of sleep timing appeared normal in BTBR mice, but there

was a significant interaction between genotype and time of day for wake and REM amounts (Fig 2B). However, these slight differences cannot explain the reversal of the E/I oscillation in BTBR mice, since BTBR mice slept primarily during the dark phase. We also examined sleep quality in each genotype (Fig. S2B-E). First, we compared the mean bout duration for each arousal state. We observed significant differences between the light and dark phases, but no differences due to genotype in *Fmr1* KO mice. BTBR mice had significantly longer REM bouts during both the light and dark phases. We also compared the number of bouts and sleep-wake transitions between genotypes, which differed significantly between the light and dark phases but not between genotypes. We observed slight but significant alterations in spectral power during sleep, most notably decreased NREM delta power in both models and increased REM theta power in BTBR mice compared to WT controls (Fig. S2E). We also observed a strong trend towards increased waking gamma power in *Fmr1* KO mice (Fig. S2F), consistent with previous reports (Goswami et al., 2019; Lovelace et al., 2018; Sinclair et al., 2017).

Both excitation and inhibition are dysregulated in two mouse models of ASD.

Our findings indicate that the E/I ratio is dysregulated across the day in two mouse models of autism. However, these data do not reveal whether excitation, inhibition, or both are responsible for this dysregulation. To determine this, we measured excitatory and inhibitory postsynaptic currents (mEPSCs, mIPSCs) in V1 layer 2/3 at ZT0 and ZT12. In *Fmr1* WT mice, mEPSC frequency was higher at ZT0 and mIPSC frequency was higher at ZT12 (Fig. 3A, B; Table S1) in accordance with previous findings (Bridi et al., 2020). In contrast, mEPSC and mIPSC frequency in *Fmr1* KO mice did not show time-of-day differences (Fig. 3A, B; Table S1), indicating that the dysregulation of the E/I ratio is caused by dysregulation of both excitatory and inhibitory synaptic transmission. No time-of-day differences in amplitude, or recording conditions were observed for either mEPSCs or mIPSCs (Fig. 3; Table S1).

We performed the same experiment for BTBR and B6 control mice. In BTBR mice, both mEPSC and mIPSC frequency showed the opposite pattern compared to B6 mice: mEPSC frequency was lower (Fig. 4A) and mIPSC frequency was higher (Fig. 4B) at ZT0 than at ZT12. There were no differences in amplitude, recording conditions, or kinetics (Fig. 4, Table S2). These results demonstrate that alterations to both excitatory and inhibitory synaptic signaling underlie the dysregulation of the E/I ration in BTBR mice.

DISCUSSION

In this study, we show that the daily E/I oscillation is dysregulated in two mouse models of ASD. The oscillation is flattened in *Fmr1* KO and phase-shifted in BTBR mice. This cannot be explained by altered sleep timing, which is essentially normal. In these two lines, the daily oscillations excitatory and inhibitory synaptic transmission are both altered, and both track the changes in E/I ratio, raising the possibility that the disruption of a deeper regulatory mechanism is common to models of ASD.

Implications across ASD models and brain regions

In WT mice, the E/I ratio and correlations between ionic conductances vary over the 24h day, indicating extensive rearrangement of connectivity and function on this timescale under normal conditions (Bridi et al., 2020; Tran et al., 2019). Therefore, it is crucial to consider ASD models against a backdrop of changing circuit properties in WT mice. If the E/I ratio in an ASD model is found to be altered at a single time of day, multiple scenarios are possible, as illustrated in Fig. S3. For example, a higher E/I ratio is consistent with elevation across all times of day (Fig. S3, orange). This is the predominant interpretation of studies reporting increased E/I ratio in sensory cortices (Antoine et al., 2019; Banerjee et al., 2016; Bridi et al., 2017; Cellot and Cherubini, 2014; Chao et al., 2010; Gibson et al., 2008; Wallace et al., 2012; Zhang et al., 2014; Zhao and Yoshii, 2019). However, a higher E/I ratio sampled at a single time point is also consistent with dysregulation by flattening (Fig. S3, green) or phase-shifting (Fig. S3, blue), scenarios we observed in *Fmr1* KO and BTBR mice, respectively. In the case of dysregulation, the overall E/I ratio may not be different between genotypes and, in fact, is the same as WT controls at two times of day. Importantly, if experiments are conducted during the light phase (when the E/I ratio is low in WT animals), studies will be predisposed to report a higher E/I ratio in ASD model genotypes when there may not be an overall difference. The model we propose in this study provides a novel viewpoint: ASD model mice may have an E/I ratio that is normal, but at inappropriate times of day. This may result in a mismatch with the animal's behavioral state that causes abnormal behavioral phenotypes.

This model is compatible with studies of V1 layer 2/3 pyramidal cells in several ASD mouse lines. mIPSC frequency is decreased in *Cntnap2*-, *Tsc1-,* and *Ube3a*-deficient mice (Bridi et al., 2017; Wallace et al., 2012; Zhao and Yoshii, 2019), although this decrease was not seen in *Fmr1* KO mice (Zhong et al., 2018). Furthermore, the visually evoked E/I ratio is elevated and inhibitory interneuron activity is decreased in *Mecp2* KO and *Fmr1* KO mice, respectively, *in vivo* (Banerjee et al., 2016; Goel et al., 2018). These findings are consistent with dysregulation resulting in higher E/I ratio during the light phase. Importantly, decreased inhibitory interneuron activity has been linked to impairments in visual discrimination, supporting the theory that dysregulation could result in behavioral impairment (Goel et al., 2018).

In WT mice, hippocampal CA1 and medial prefrontal cortex undergo the same pattern of daily E/I oscillation as V1 (Bridi et al., 2020), raising the possibility that the dysregulation we observed in *Fmr1* KO and BTBR mice may extend to other brain regions. In support of this idea, in CA1, spontaneous IPSC frequency is lower in both lines (Cellot et al., 2016; Han et al., 2014; Sabanov et al., 2017), the evoked E/I ratio is elevated in the temporoammonic pathway of *Fmr1* KO mice (Wahlstrom-Helgren and Klyachko, 2015) and sEPSC frequency is increased in BTBR mice (Han et al., 2014). Similarly, in insular cortex layer 2/3, mISPC frequency is lower in

BTBR than WT mice (Gogolla et al., 2014). These findings are consistent with dysregulation across regions in both models, as flattening in *Fmr1* KO and phase shifting in BTBR mice would both result in an elevated E/I ratio during the light phase. On the other hand, alterations have been reported in CA1 that cannot be explained by dysregulation, including changes in spontaneous and miniature E/IPSC amplitude, which do not oscillate across the day in WT mice (Bridi et al., 2020; Han et al., 2014; Sabanov et al., 2017). Furthermore, different patterns may emerge in distinct subregions of the hippocampus, as sIPSC frequency and amplitude are elevated in the CA3 region of BTBR mice (Cellot et al., 2016). Together, this suggests that E/I dysregulation likely extends beyond V1, but may not be the only factor contributing to E/I ratio disruption in these areas.

The E/I ratio oscillation occurs in multiple brain regions, but is not uniform across cortical circuits. In WT mice, the E/I ratio in V1 is labile in the layer 2/3-2/3 but fixed in the layer 4-2/3 circuit over the 24h day (Fig. 1, S1; Bridi et al., 2020). Here, we show that the E/I ratio remains fixed in the layer 4-2/3 circuit of both *Fmr1* KO and BTBR mice. Moreover, we did not observe a general elevation of the E/I ratio in the layer 4-2/3 circuit of V1 in either line (Fig. S2). However, our findings in V1 contrast with other sensory cortices. In S1 of *Fmr1* KO mice, the E/I ratio is elevated in the layer 4-2/3 circuit, and inhibition is decreased in the local S1 layer 4-4 circuit (Antoine et al., 2019; Gibson et al., 2008). Whether these discrepancies are due to the E/I oscillation occurring in different circuits in S1 compared to V1 remains to be seen.

Candidate Mechanisms of E/I dysregulation

Sleep disruption is a common feature of autism (reviewed in Schreck and Richdale, 2020), and controls the daily oscillation of inhibition (Bridi et al., 2020). Although we detected some minor differences in sleep architecture, sleep timing follows a grossly normal pattern of nocturnal activity in *Fmr1* KO and BTBR mice, consistent with previous studies in *Fmr1* mice using video recording and wheel running (Saré et al., 2017; Zhang et al., 2008). Furthermore, despite a variety of altered sleep/activity characteristics, a basically normal nocturnal activity pattern in preserved across many other commonly used ASD models including 16p11.2 deletion, *Cntnap2* KO, *Mecp2*-deficient, *Nlgn1* KO, *Nlgn2* KO, *Nlgn*3^{R451C}, *Shank3*$^{\Delta C}$, *Tsc1*/*Tsc2* deficient, and *Ube3a* KO mice (Angelakos et al., 2017; Colas et al., 2005; Ehlen et al., 2015; El Helou et al., 2013; Ingiosi et al., 2019; Johnston et al., 2014; Li et al., 2015; Lipton et al., 2017; Liu et al., 2017; Lu et al., 2019; Seok et al., 2018; Thomas et al., 2017; Tsuchiya et al., 2015; Wither et al., 2012). Therefore, dysregulation of the E/I ratio is unlikely to arise from altered sleep timing in *Fmr1* KO or BTBR mice, and in ASD model mice more broadly. We did detect small differences in sleep architecture of BTBR mice (Fig 2, S2), but these minor differences are unlikely to be responsible for the dramatic phase-reversal in E/I ratio that we observed (Fig. 1, 4). We did not replicate previously reported deficits in REM sleep in *Fmr1* KO mice (Boone et al., 2018), which may be due to the use of younger mice in the present study. A significant decrease in sleep during the light phase emerges sometime between 3 and 10 weeks of age in *Fmr1* KO mice (Saré et al., 2017), which could be due to loss of REM sleep time. Therefore, recordings in the current study (at 5-8 weeks of age) may have preceded the developmental appearance of a REM deficit.

We also examined spectral characteristics of sleep and wake states in *Fmr1* KO and BTBR mice. We observed a strong trend toward increased gamma power during waking in *Fmr1* KO,

but not BTBR mice, consistent with previous reports in mice (Goswami et al., 2019; Lovelace et al., 2018; Sinclair et al., 2017) and humans (Wang et al., 2017). We also observed decreased power in the delta (0.5-1 Hz) frequency range during NREM sleep in both genotypes, consistent with reports in a number of other ASD mouse lines (Angelakos et al., 2017; Ehlen et al., 2015; Ingiosi et al., 2019; Johnston et al., 2014; Liu et al., 2017; Lu et al., 2019), suggesting that poor quality NREM sleep could contribute to E/I dysregulation.

Two additional potential mechanisms underlying E/I dysregulation are endocannabinoid (eCB) signaling and homeostasis. The eCB system is postulated to be disrupted in individuals with ASD (reviewed in Chakrabarti et al., 2015), and eCB signaling regulates the daily oscillation of inhibitory transmission in WT mice (Bridi et al., 2020). This raises the possibility that disruption of eCB signaling may underlie E/I dysregulation in ASD mouse lines, and is an important focus of future work. Second, it has been proposed that altered excitatory and inhibitory synaptic transmission may not be a primary effect of the ASD phenotype, but rather reflect homeostatic compensation (Nelson and Valakh, 2015). In support of this idea, an elevated E/I ratio homeostatically regulates neuronal firing in S1 of *Fmr1* KO mice (Antoine et al., 2019). Here, we find that E/I dysregulation is carried by altered oscillation of both excitatory and inhibitory synaptic transmission, changes that could be driven by homeostatic mechanisms to maintain the oscillation of circuit excitability observed in WT mice (Bridi et al., 2020).

The current study reformulates our view of the E/I ratio in ASD. The E/I ratio is a labile property in specific circuits, and these circuits may be more vulnerable to dysfunction because multiple mechanisms control the E/I oscillation and have the potential to be disrupted. Targeting future studies to these circuits and incorporating time of day as a factor may reconcile discrepancies within and across ASD models. This will produce a more unified picture of ASD pathophysiology, and potentially provide insight into treatment plans that may improve behavioral outcomes in affected individuals.

FIGURE LEGENDS:

Figure 1. E/I is dysregulated in two mouse models of autism. (A) Left: *Fmr1* KO/WT (green) and BTBR/B6 (blue) mice were sacrificed at the indicated times of day. Right: Acute brain slices containing V1 were obtained, and responses to layer 2/3 stimulation over a range of intensities were recorded using whole-cell patch clamp of layer 2/3 pyramidal neurons. Inhibitory (upward deflection) and excitatory (downward deflection) responses were recorded in the same cell and the E/I ratio was calculated using the stimulation intensities over which the E/I ratio was stable (Bridi et al., 2020). (B) Oscillation of the E/I ratio across the day is absent in *Fmr1* KO mice. Top: *Fmr1* KO Kruskal-Wallis $H_{(3,\ 102)}$=1.62, P=0.65. Bottom: *Fmr1* WT 1-way ANOVA $F_{(3,\ 94)}$=6.67, P=0.0004; Holm-Sidak post-hoc test P values indicated. (C) BTBR mice exhibit a phase-shifted E/I oscillation, such that the E/I ratio is high at ZT12, contrasting with higher E/I at ZT0 in B6 mice. Top: BTBR 2-tailed t test $t_{(45)}$=2.64; Bottom: B6 2-tailed t test $t_{(41)}$=2.93. For all panels, sample size is indicated as (cells, mice). Error bars indicate mean±SEM. Example traces are normalized to peak inhibitory response.

Figure 2. Sleep timing is normal in *Fmr1* KO and BTBR mice. (A) Percent time *Fmr1* mice spent awake (A_1), in NREM sleep (A_2), and in REM sleep (A_3). There was no significant main effect of genotype for any arousal state (%W $F_{(1,\ 12)}$=3.43, P=0.09, %NREM $F_{(1,\ 12)}$=2.80, P=0.12, %REM $F_{(1,\ 12)}$=0.86, P=0.37). There was also no significant genotype × time of day interaction when data were broken into 1h bins (left) (%W $F_{(23,\ 276)}$=0.88, P=0.63, %NREM $F_{(23,\ 276)}$=0.88, P=0.63, %REM $F_{(23,\ 276)}$=0.76, P=0.78) or averaged across the 12-h light and dark phases (right) (%W $F_{(1,\ 12)}$=3.12, P=0.10, %NREM $F_{(1,\ 12)}$=3.23, P=0.09, %REM $F_{(1,\ 12)}$=1.81, P=0.20). There was a significant main effect of time for all states (%W: $F_{(1,\ 12)}$=153.0, P<0.0001; %NREM: $F_{(1,\ 12)}$=162.9, P<0.0001; %REM: $F_{(1,\ 12)}$=85.6, P<0.0001). (B) Percent time BTBR and B6 mice spent in each arousal state. BTBR mice displayed grossly normal sleep timing (i.e. slept more during the dark phase) and there was no significant main effect of genotype for any arousal state (%W $F_{(1,\ 14)}$=0.72, P=0.41, %NREM $F_{(1,\ 14)}$=0.48, P=0.50, %REM $F_{(1,\ 14)}$=0.54, P=0.47). There were small but significant interaction effects for wake (B_1) and REM sleep (B_3) when data were broken into 1h bins (left) (%W $F_{(23,\ 322)}$=1.57, P=0.048, %NREM $F_{(23,322)}$=1.521, P=0.06, %REM $F_{(23,\ 322)}$=2.05, P=0.0035) and for REM sleep (B_3) when data were averaged into 12h bins (right) (%W $F_{(1,\ 14)}$=2.39, P=0.24, %NREM $F_{(1,\ 14)}$=1.95, P=0.18, %REM $F_{(1,\ 14)}$=4.93, P=0.04). There was a main time of day effect for all states (%W $F_{(1,\ 14)}$=258.9, P<0.0001, %NREM $F_{(1,\ 14)}$=232.0, P<0.0001, %REM $F_{(1,\ 14)}$=342.5, P<0.0001). Data were averaged over 3 recording days for each mouse prior to statistical analysis. All data were analyzed using 2-way repeated measures ANOVAs. Data are shown as mean ± SEM. N=number of mice.

Figure 3. Oscillation of both excitation and inhibition is flattened in *Fmr1* KO mice. (A) mEPSC frequency does not change with time of day in *Fmr1* KO mice (U=613, P=0.35, Mann-Whitney test), but is higher at ZT0 in *Fmr1* WT control mice (U=269, P=0.001, Mann-Whitney test). Amplitude did not change with time of day in either genotype (KO: U=579, P=0.19; WT: U=445, P=0.39; Mann-Whitney test). (B) mIPSC frequency does not change with time of day in *Fmr1* KO mice (U=596, P=0.93, Mann-Whitney test), but is higher at ZT12 in *Fmr1* WT control mice ($t_{(51)}$=2.69, P=0.0098, t test). Amplitude did not change with time of day in either genotype (KO: $t_{(68)}$=1.26, P=0.21; WT: $t_{(51)}$=0.46, P=0.65, t test). Data are presented as mean±SEM. Sample size is indicated as (cells, mice). Averaged traces: solid lines indicate ZT0, dotted lines indicate ZT12; scaled, superimposed averaged traces illustrate that there was no difference in kinetics between the two times of day (Table S1).

Figure 4. Oscillation of both excitation and inhibition is reversed in BTBR mice. (A) mEPSC frequency is higher at ZT12 in BTBR mice (U=322, P=0.016, Mann-Whitney test), and higher at ZT0 in B6 control mice ($t_{(67)}$=2.53, P=0.014, t test). Amplitude did not change with time of day in either genotype (BTBR: $t_{(61)}$=1.08, P=0.28; B6: $t_{(67)}$=0.11, P=0.91; t test). (B) mIPSC frequency is higher at ZT0 in BTBR mice (U=278, P=0.026, Mann-Whitney test), and higher at ZT12 in B6 controls (U=464, P=0.017, Mann-Whitney test). Amplitude did not change with time of day in either genotype (BTBR: $t_{(56)}$=0.93, P=0.36; B6: $t_{(72)}$=1.71, P=0.09, t test). Data are presented as mean±SEM. Sample size is indicated as (cells, mice). Averaged traces: solid lines indicate ZT0, dotted lines indicate ZT12; scaled, superimposed averaged traces illustrate that there was no difference in kinetics between the two times of day (Table S2).

REFERENCES

Angelakos, C.C., Watson, A.J., O'Brien, W.T., Krainock, K.S., Nickl-Jockschat, T., and Abel, T. (2017). Hyperactivity and male-specific sleep deficits in the 16p11.2 deletion mouse model of autism. Autism Res *10*, 572–584.

Antoine, M.W., Langberg, T., Schnepel, P., and Feldman, D.E. (2019). Increased excitation-inhibition ratio stabilizes synapse and circuit excitability in four autism mouse models. Neuron *101*, 648–661.

Bakker, C.E., Verheij, C., Willemsen, R., van der Helm, R., Oerlemans, F., Vermey, M., Bygrave, A., Hoogeveen, A.T., Oostra, B.A., Reyniers, E., et al. (1994). Fmr1 knockout mice : A model to study fragile X mental retardation. Cell *78*, 23–33.

Banerjee, A., Rikhye, R. V, Breton-Provencher, V., Tang, X., Li, C., Li, K., Runyan, C.A., Fu, Z., Jaenisch, R., and Sur, M. (2016). Jointly reduced inhibition and excitation underlies circuit-wide changes in cortical processing in Rett syndrome. Proc Natl Acad Sci U S A *113*, E7287–E7296.

Boone, C.E., Davoudi, H., Harrold, J.B., and Foster, D.J. (2018). Abnormal sleep architecture and hippocampal circuit dysfunction in a mouse model of fragile X syndrome. Neuroscience *384*, 275–289.

Bridi, M.C.D., Zong, F.-J., Min, X., Luo, N., Tran, T., Qiu, J., Severin, D., Zhang, X.-T., Wang, G., Zhu, Z.-J., et al. (2020). Daily oscillation of the excitation-inhibition balance in visual cortical circuits. Neuron *105*, 621–629.

Bridi, M.S., Park, S.M., and Huang, S. (2017). Developmental disruption of GABAAR-meditated inhibition in Cntnap2 KO mice. ENeuro *4*, e0162–17.2017.

Cellot, G., and Cherubini, E. (2014). Reduced inhibitory gate in the barrel cortex of Neuroligin3 R451C knock-in mice , an animal model of autism spectrum disorders. Physiol Rep *2*, e12077.

Cellot, G., Maggi, L., Di Castro, M.A., Catalano, M., Migliore, R., Migliore, M., Scattoni, M.L., Calamandrei, G., and Cherubini, E. (2016). Premature changes in neuronal excitability account for hippocampal network impairment and autistic-like behavior in neonatal BTBR T+tf/J mice. Sci Rep *6*, 31696.

Chakrabarti, B., Persico, A., Battista, N., and Maccarrone, M. (2015). Endocannabinoid signaling in autism. Neurotherapeutics *12*, 837–847.

Chao, H.-T., Chen, H., Samaco, R.C., Xue, M., Chahrour, M., Yoo, J., Neul, J.L., Gong, S., Lu, H., Heintz, N., et al. (2010). Dysfunction in GABA signalling mediates autism-like stereotypies and Rett syndrome phenotypes. Nature *468*, 263–296.

Colas, D., Wagstaff, J., Fort, P., Salvert, D., and Sarda, N. (2005). Sleep disturbances in Ube3a maternal-deficient mice modeling Angelman syndrome. Neurobiol Dis *20*, 471–478.

Dani, V.S., Chang, Q., Maffei, A., Turrigiano, G.G., Jaenisch, R., and Nelson, S.B. (2005). Reduced cortical activity due to a shift in the balance between excitation and inhibition in a mouse model of Rett Syndrome. Proc Natl Acad Sci U S A *102*, 12560–12565.

Delattre, V., La Mendola, D., Meystre, J., Markram, H., and Markram, K. (2013). Nlgn4 knockout induces network hypo-excitability in juvenile mouse somatosensory cortex in vitro. Sci Rep *3*, 2897.

Ehlen, J.C., Jones, K.A., Pinckney, L., Gray, C.L., Burette, S., Weinberg, R.J., Evans, J.A., Brager, A.J., Zylka, M.J., Paul, K.N., et al. (2015). Maternal Ube3a loss disrupts sleep homeostasis but leaves circadian rhythmicity largely intact. J Neurosci *35*, 13587–13598.

Etherton, M., Földy, C., Sharma, M., Tabuchi, K., Liu, X., Shamloo, M., Malenka, R.C., and Sudhof, T.C. (2011). Autism-linked neuroligin-3 R451C mutation differentially alters hippocampal and cortical synaptic function. Proc Natl Acad Sci U S A *108*, 13764–13769.

Geschwind, D.H. (2009). Advances in autism. Annu Rev Med *60*, 367–380.

Gibson, J.R., Bartley, A.F., Hays, S.A., and Huber, K.M. (2008). Imbalance of neocortical excitation and inhibition and altered UP states reflect network hyperexcitability in the mouse model of fragile X syndrome. J Neurophysiol *100*, 2615–2626.

Goel, A., Cantu, D.A., Guilfoyle, J., Chaudhari, G.R., Newadkar, A., Todisco, B., de Alba, D., Kourdougli, N., Schmitt, L.M., Pedapati, E., et al. (2018). Impaired perceptual learning in a mouse model of Fragile X syndrome is mediated by parvalbumin neuron dysfunction and is reversible. Nat Neurosci *21*, 1404–1411.

Gogolla, N., Takesian, A.E., Feng, G., Fagiolini, M., and Hensch, T.K. (2014). Sensory integration in mouse insular cortex reflects GABA circuit maturation. Neuron *83*, 894–905.

Goswami, S., Cavalier, S., Sridhar, V., Huber, K.M., and Gibson, J.R. (2019). Local cortical circuit correlates of altered EEG in the mouse model of Fragile X syndrome. Neurobiol Dis *124*, 563–572.

Hagerman, R.J., Berry-Kravis, E., Hazlett, H.C., Bailey, D.B.J., Moine, H., Kooy, R.F., Tassone, F., Gantois, I., Sonenberg, N., Mandel, J.L., et al. (2017). Fragile X syndrome. Nat Rev Dis Prim *3*, 17065.

Han, S., Tai, C., Jones, C.J., Scheuer, T., and Catterall, W.A. (2014). Enhancement of inhibitory neurotransmission by GABAA receptors having α2,3 -subunits ameliorates behavioral deficits in a mouse model of autism. Neuron *81*, 1282–1289.

Harrington, A.J., Raissi, A., Rajkovich, K., Berto, S., Kumar, J., Molinaro, G., Raduazzo, J., Guo, Y., Loerwald, K., Konopka, G., et al. (2016). MEF2C regulates cortical inhibitory and excitatory synapses and behaviors relevant to neurodevelopmental disorders. Elife *5*, e20059.

El Helou, J., Bélanger-nelson, E., Freyburger, M., Dorsaz, S., and Curie, T. (2013). Neuroligin-1 links neuronal activity to sleep-wake regulation. Proc Natl Acad Sci USA *110*, 9974–9979.

Ingiosi, A.M., Schoch, H., Wintler, T., Singletary, K.G., Righelli, D., Roser, L.G., Medina, E., Risso, D., Frank, M.G., and Peixoto, L. (2019). Shank3 modulates sleep and expression of circadian transcription factors. Elife *8*, e42819.

Johnston, M. V, Ammanuel, S., O'Driscoll, C., Wozniak, A., Naidu, S., and Kadam, S.D. (2014). Twenty-four hour quantitative-EEG and in-vivo glutamate biosensor detects activity and circadian rhythm dependent biomarkers of pathogenesis in Mecp2 null mice. Front Sytems Neurosci *8*, 1–13.

Li, Q., Loh, D.H., Kudo, T., Truong, D., Derakhshesh, M., Macdowell, Z., Ghiani, C.A., Tsoa, R., Cheng, Y., Sun, Y.E., et al. (2015). Circadian rhythm disruption in a mouse model of Rett syndrome circadian disruption in RTT. Neurobiol Dis *77*, 155–164.

Lipton, J.O., Boyle, L.M., Yuan, E.D., Hochstrasser, K.J., Chifamba, F.F., Nathan, A., Tsai, P.T., Davis, F., and Sahin, M. (2017). Aberrant proteostasis of BMAL1 underlies circadian

abnormalities in a paradigmatic mTOR-opathy. Cell Rep *20*, 868–880.

Liu, J.J., Grace, K.P., Horner, R.L., Cortez, M.A., Shao, Y., and Jia, Z. (2017). Neuroligin 3 R451C mutation alters electroencephalography spectral activity in an animal model of autism spectrum disorders. Mol Brain *10*, 10.

Liu, Z.-W., Faraguna, U., Cirelli, C., Tononi, G., and Gao, X.-B. (2010). Direct evidence for wake-related increases and sleep-related decreases in synaptic strength in rodent cortex. J Neurosci *30*, 8671–8675.

Lovelace, J.W., Ethell, I.M., Binder, D.K., and Razak, K.A. (2018). Translation-relevant EEG phenotypes in a mouse model of Fragile X Syndrome. Neurobiol Dis *115*, 39–48.

Lu, H.-C., Pollack, H., Lefante, J.J., Mills, A.A., and Tian, D. (2019). Altered sleep architecture, rapid eye movement sleep, and neural oscillation in a mouse model of human chromosome 16p11.2 microdeletion. Sleep *42*, zsy253.

Maenner, M.J., Shaw, K.A., Baio, J., Washington, A., Patrick, M., DiRienze, M., Christensen, D.L., Wiggins, L.D., Pettygrove, S., Andrews, J.G., et al. (2020). Prevalence of autism spectrum disorder among children aged 8 years — Autism and developmental disabilities monitoring network , 11 sites , United States , 2016. MMWR Surveill Summ *69*, 1–12.

McFarlane, H.G., Kusek, G.K., Yang, M., Phoenix, J.L., Bolivar, V.J., and Crawley, J.N. (2008). Autism-like behavioral phenotypes in BTBR T+tf/J mice. Genes Brain Behav *7*, 152–163.

Meyza, K.Z., and Blanchard, D.C. (2017). The BTBR mouse model of idiopathic autism – Current view on mechanisms. Neurosci Biobehav Rev *76*, 99–110.

Nelson, S.B., and Valakh, V. (2015). Excitatory/inhibitory balance and circuit homeostasis in autism spectrum disorders. Neuron *87*, 684–698.

Robertson, C.E., and Baron-Cohen, S. (2017). Sensory perception in autism. Nat Rev Neurosci *18*, 671–684.

Rubenstein, J.L.R., and Merzenich, M.M. (2003). Model of autism : Increased ratio of excitation / inhibition in key neural systems. Genes Brain Behav *2*, 255–267.

Sabanov, V., Braat, S., D'Andrea, L., Willemsen, R., Zeidler, S., Rooms, L., Bagni, C., Kooy, R.F., and Balschun, D. (2017). Impaired GABAergic inhibition in the hippocampus of Fmr1 knockout mice. Neuropharmacology *116*, 71–81.

Saré, R.M., Harkless, L., Levine, M., Torossian, A., Sheeler, C.A., and Smith, C.B. (2017). Deficient sleep in mouse models of fragile X syndrome. Front Mol Neurosci *10*, 280.

Schreck, K.A., and Richdale, A.L. (2020). Sleep problems, behavior, and psychopathology in autism: inter-relationships across the lifespan. Curr Opin Psychol *34*, 105–111.

Seok, B.S., Bélanger-Nelson, E., Provost, C., Gibbs, S., and Mongrain, V. (2018). The effect of Neuroligin-2 absence on sleep architecture and electroencephalographic activity in mice. Mol Brain *11*, 1–11.

Sinclair, D., Featherstone, R., Naschek, M., Nam, J., Du, A., Wright, S., Pance, K., Weger, R., Akuzawa, S., Matsumoto, M., et al. (2017). GABA-B agonist baclofen normalizes auditory-evoked neural oscillations and behavioral deficits in the Fmr1 knockout mouse model of Fragile X syndrome. eNeuro *4*, 1–13.

Tabuchi, K., Blundell, J., Etherton, M.R., Hammer, R.E., Liu, X., Powell, C.M., and Südhof, T.C.

(2007). A neuroligin-3 mutation implicated in autism increases inhibitory synaptic transmission in mice. Science *318*, 71–76.

Thomas, A.M., Schwartz, M.D., Saxe, M.D., and Kilduff, T.S. (2017). Cntnap2 knockout rats and mice exhibit epileptiform activity and abnormal sleep-wake physiology. Sleep *40*, 1–14.

Tran, T., Unal, C.T., Severin, D., Zaborszky, L., Rotstein, H.G., Kirkwood, A., and Golowasch, J. (2019). Ionic current correlations are ubiquitous across phyla. Sci Rep *9*, 1687.

Tsuchiya, Y., Minami, Y., Umemura, Y., Watanabe, H., Ono, D., Nakamura, W., Takahashi, T., Honma, S., Kondoh, G., Matsuishi, T., et al. (2015). Disruption of MeCP2 attenuates circadian rhythm in CRISPR/Cas9-based Rett syndrome model mouse. Genes Cells *20*, 992–1005.

Unichenko, P., Yang, J., Kirischuk, S., Kolbaev, S., Kilb, W., Hammer, M., Krueger-Burg, D., Brose, N., and Luhmann, H.J. (2018). Autism related neuroligin-4 knockout impairs intracortical processing but not sensory inputs in mouse barrel cortex. Cereb Cortex *28*, 2873–2886.

Wahlstrom-Helgren, S., and Klyachko, V.A. (2015). GABAB receptor-mediated feed-forward circuit dysfunction in the mouse model of fragile X syndrome. J Physiol *593*, 5009–5024.

Wallace, M.L., Burette, A.C., Weinberg, R.J., and Philpot, B.D. (2012). Maternal loss of Ube3a produces an excitatory/inhibitory imbalance through neuron type-specific synaptic defects. Neuron *74*, 793–800.

Wang, J., Ethridge, L.E., Mosconi, M.W., White, S.P., Binder, D.K., Pedapati, E. V, Erickson, C.A., Byerly, M.J., and Sweeney, J.A. (2017). A resting EEG study of neocortical hyperexcitability and altered functional connectivity in fragile X syndrome. J Neurodev Disord *9*, 1–12.

Wither, R.G., Colic, S., Wu, C., Bardakjian, B.L., Zhang, L., and Eubanks, J.H. (2012). Daily rhythmic behaviors and thermoregulatory patterns are disrupted in adult female MeCP2-deficient mice. PLoS One *7*, e35396.

Zhang, J., Fang, Z., Jud, C., Vansteensel, M.J., Kaasik, K., Lee, C.C., Albrecht, U., Tamanini, F., Meijer, J.H., Oostra, B.A., et al. (2008). Fragile X-related proteins regulate mammalian circadian behavioral rhythms. Am J Hum Genet *83*, 43–52.

Zhang, W., Peterson, M., Beyer, B., Frankel, W.N., and Zhang, Z. (2014). Loss of MeCP2 from forebrain excitatory neurons leads to cortical hyperexcitation and seizures. J Neurosci *34*, 2754–2763.

Zhao, J.-P., and Yoshii, A. (2019). Hyperexcitability of the local cortical circuit in mouse models of tuberous sclerosis complex. Mol Brain *12*, 1–13.

Zhong, L.R., Chen, X., Park, E., Sudhof, T.C., and Chen, L. (2018). Retinoic acid receptor RAR alpha-dependent synaptic signaling mediates homeostatic synaptic plasticity at the inhibitory synapses of mouse visual cortex. J Neurosci *38*, 10454–10466.

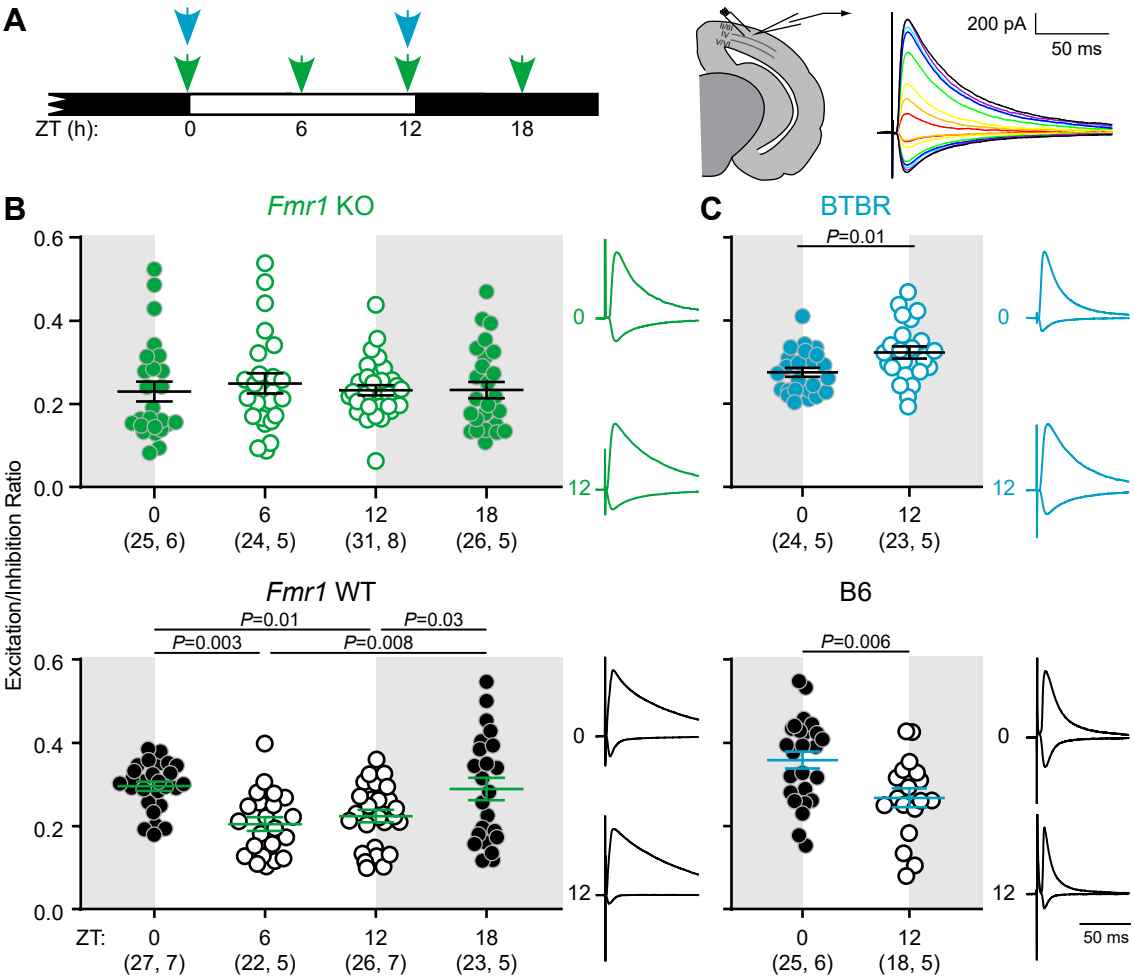
A
ZT (h):
0
6
12
18
200 pA
50 ms
B
Fmr1 KO
C
BTBR
P=0.01
Excitation/Inhibition Ratio
0.6
0.4
0.2
0.0
0
(25, 6)
6
(24, 5)
12
(31, 8)
18
(26, 5)
0
(24, 5)
12
(23, 5)
Fmr1 WT
B6
P=0.01
P=0.03
P=0.003
P=0.008
P=0.006
ZT:
(27, 7)
(22, 5)
(26, 7)
(23, 5)
(25, 6)
(18, 5)
50 ms

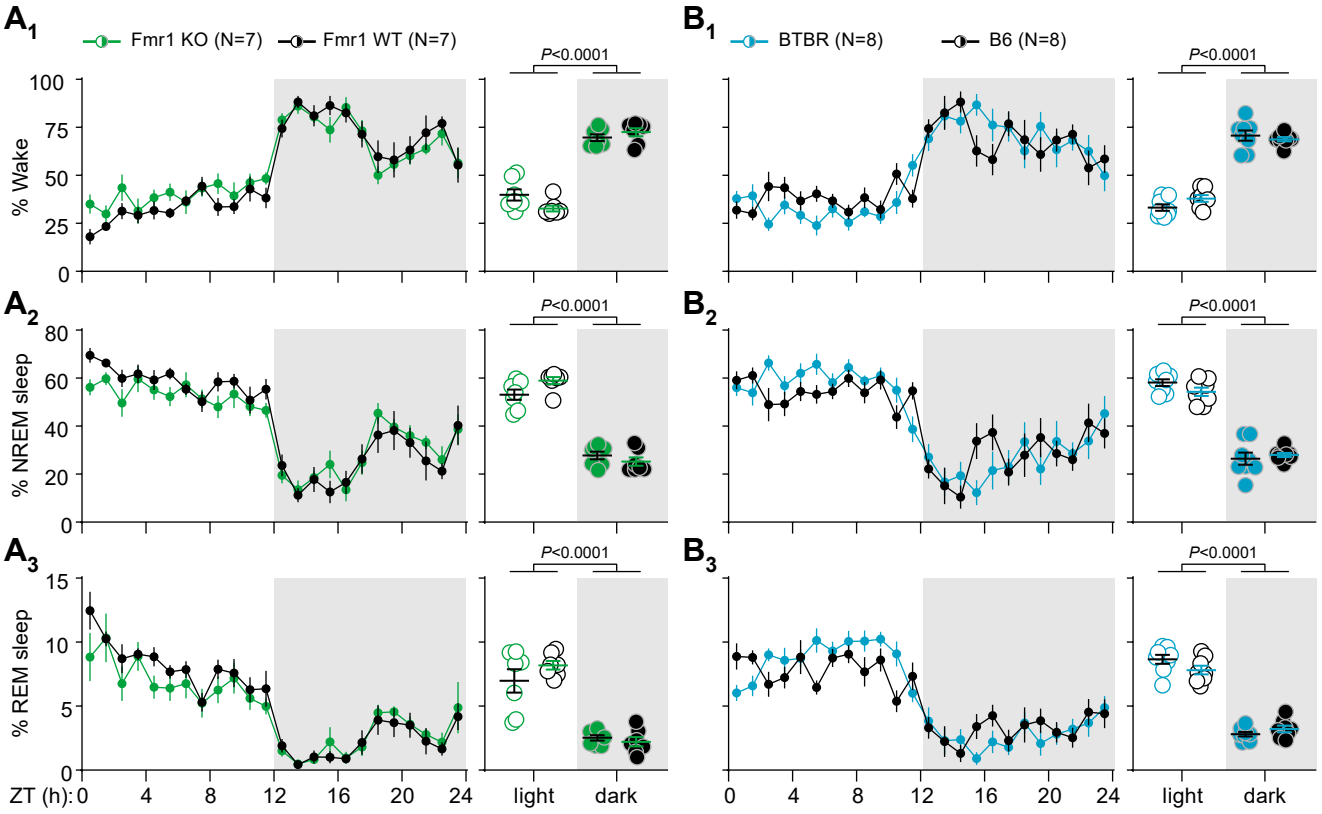
A1
Fmr1 KO (N=7)
Fmr1 WT (N=7)
B1
BTBR (N=8)
B6 (N=8)
P<0.0001
% Wake
A2
B2
% NREM sleep
A3
B3
% REM sleep
ZT (h): 0 4 8 12 16 20 24
light
dark

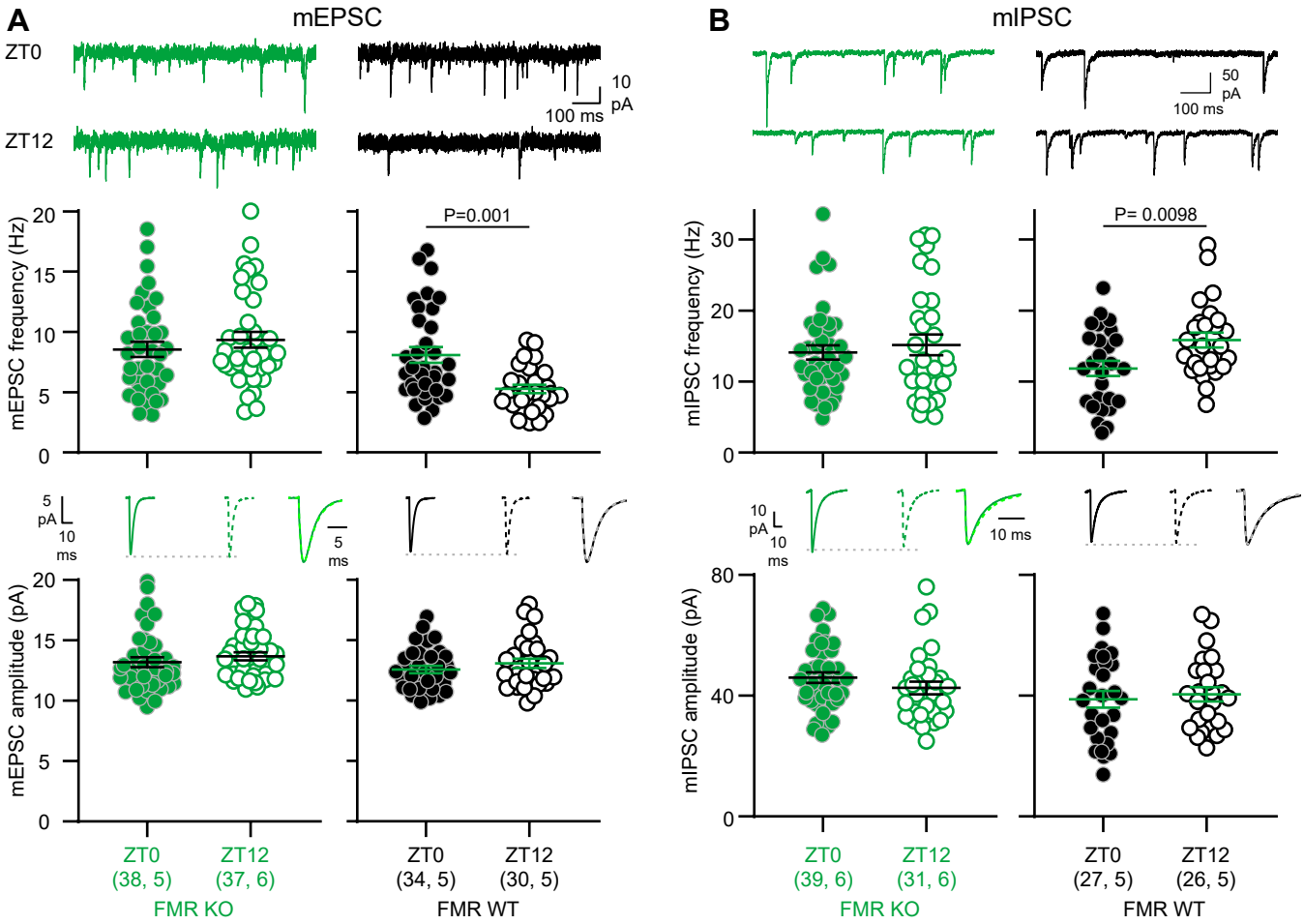
A
mEPSC
ZT0
ZT12
10 pA
100 ms
mEPSC frequency (Hz)
P=0.001
5 pA
10 ms
5 ms
mEPSC amplitude (pA)
ZT0 (38, 5)
ZT12 (37, 6)
FMR KO
ZT0 (34, 5)
ZT12 (30, 5)
FMR WT
B
mIPSC
50 pA
100 ms
mIPSC frequency (Hz)
P= 0.0098
10 pA
10 ms
10 ms
mIPSC amplitude (pA)
ZT0 (39, 6)
ZT12 (31, 6)
FMR KO
ZT0 (27, 5)
ZT12 (26, 5)
FMR WT

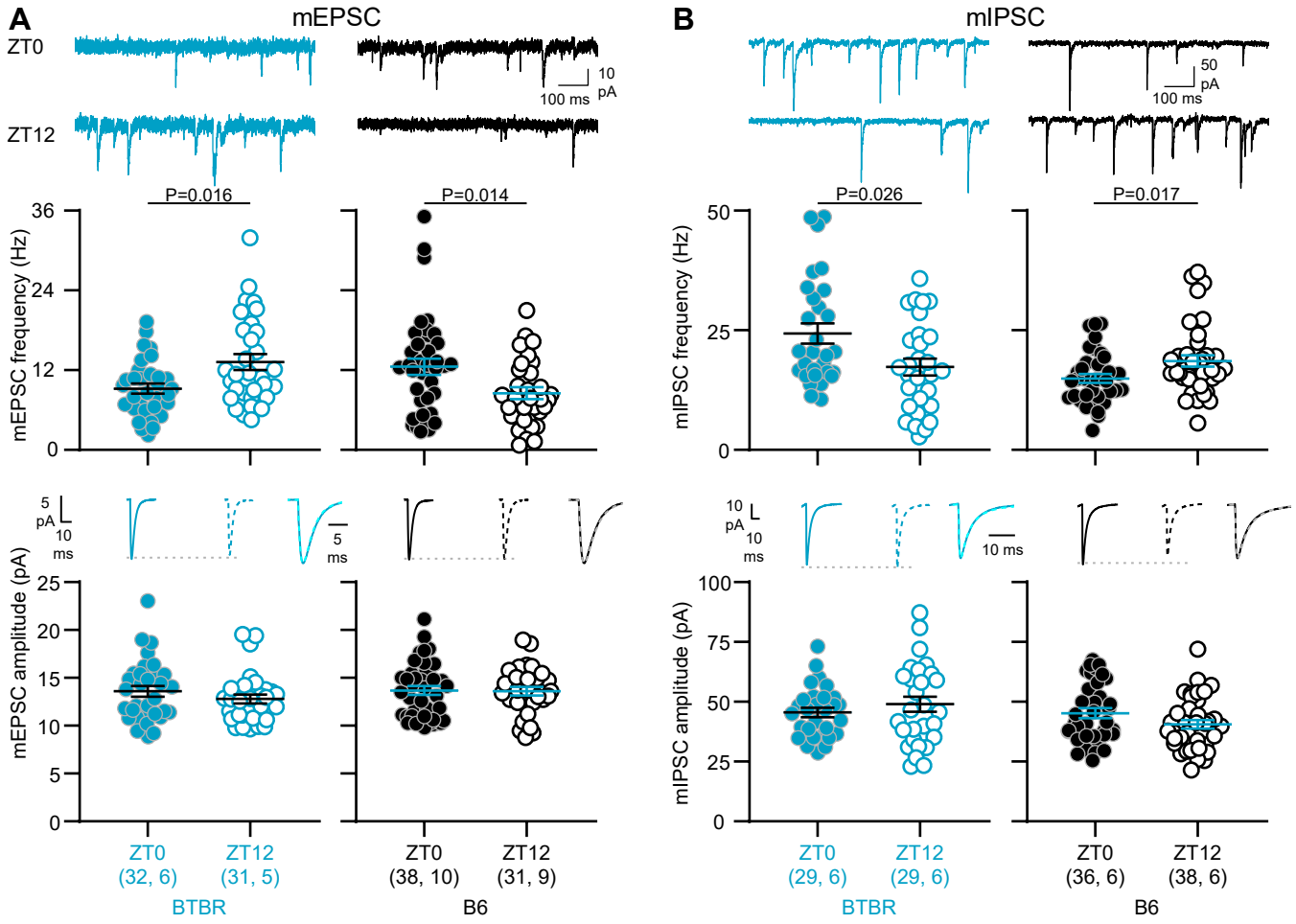
A
mEPSC
ZT0
ZT12
10 pA
100 ms
P=0.016
P=0.014
mEPSC frequency (Hz)
36
24
12
0
5 pA
10 ms
5 ms
mEPSC amplitude (pA)
25
20
15
10
5
0
ZT0 (32, 6)
ZT12 (31, 5)
BTBR
ZT0 (38, 10)
ZT12 (31, 9)
B6
B
mIPSC
50 pA
100 ms
P=0.026
P=0.017
mIPSC frequency (Hz)
50
25
0
10 pA
10 ms
10 ms
mIPSC amplitude (pA)
100
75
50
25
0
ZT0 (29, 6)
ZT12 (29, 6)
BTBR
ZT0 (36, 6)
ZT12 (38, 6)
B6

Supplementary Figure 1. The layer 4-2/3 E/I ratio is not affected by time of day. (A) *Fmr1* WT, *Fmr1* KO, B6, and BTBR mice were sacrificed at two times of day and acute brain slices containing V1 were collected for whole-cell patch clamp recordings of layer 2/3 pyramidal neurons in response to layer 4 stimulation. (B) The E/I ratio was not different between ZT0 and ZT12 in *Fmr1* KO and WT mice. Top: KO 2-tailed *t* test $t_{(28)}$=0.13, P=0.90. Bottom: WT 2-tailed *t* test $t_{(34)}$=0.22, P=0.82. When all groups were compared using a 2-way ANOVA, no significant main effect of time ($F_{(1, 62)}$=0.0002, P=0.99), genotype ($F_{(1, 62)}$=3.37, P=0.07), or time × genotype interaction ($F_{(1, 62)}$=0.05, P=0.82) was observed. (C) The E/I ratio was not different between ZT0 and ZT12 B6 and BTBR mice. Top: BTBR 2-tailed *t* test $t_{(41)}$=0.56, P=0.58. Bottom: B6 2-tailed *t* test $t_{(43)}$=1.44, P=0.16. When all groups were compared using a 2-way ANOVA, no significant main effect of time ($F_{(1, 84)}$=0.32, P=0.57), genotype ($F_{(1, 84)}$=0.08, P=0.78), or time × genotype interaction ($F_{(1, 84)}$=1.95, P=0.17) was observed. For all panels, sample size is indicated as (cells, mice). Error bars indicate mean±SEM Example traces show the inhibitory response (upward deflection) and excitatory response (downward deflection) in the same cell and are normalized to peak inhibitory response.

Supplementary Figure 2. Sleep architecture and EEG power in ASD model mice. **(A)** Overall amounts of wake, NREM sleep, and REM sleep did not differ between *Fmr1* KO and WT mice (wake: $t_{(12)}$=1.081, P=0.30; NREM: $t_{(12)}$=0.96, P=0.36, *t* test; REM: U=22, P=0.80, Mann-Whitney test), or between BTBR and B6 mice (wake: $t_{(14)}$=0.85, P=0.41; NREM: $t_{(14)}$=0.69, P=0.50; REM: $t_{(14)}$=0.73, P=0.48; *t* test). **(B)** In *Fmr1* mice, there was no effect of genotype or genotype × time interaction on bout duration for any arousal state (Wake: genotype $F_{(1,12)}$=2.67, P=0.13; interaction $F_{(1,12)}$=3.36, P=0.09; NREM: genotype $F_{(1,12)}$=2.14, P=0.17, interaction $F_{(1,12)}$=0.20, P=0.67; REM: genotype $F_{(1,12)}$=0.22, P=0.65, interaction $F_{(1,12)}$=0.004, P=0.95). Both *Fmr1* KO and WT mice had shorter wake and longer sleep bouts during the light phase (Wake: $F_{(1,12)}$=71.14, P<0.0001; NREM: $F_{(1,12)}$=61.80, P<0.0001; REM: $F_{(1,12)}$=9.41, P=0.01). BTBR mice had significantly longer REM sleep bouts than B6 mice in both the light and dark phases ($F_{(1,14)}$=6.05, P=0.03). There was also a main time of day effect for wake ($F_{(1,14)}$=71.78, P<0.0001) and REM ($F_{(1,14)}$=5.92, P=0.029) states. No genotype × time interactions were observed for any state (Wake: $F_{(1,14)}$=0.51, P=0.49; NREM: $F_{(1,14)}$=2.42, P=0.14; REM: $F_{(1,14)}$=2.54, P=0.13). All comparisons were conducted by 2-way repeated measures ANOVA. **(C)** Number of bouts/hour was higher for all arousal states during the light phase than during the dark phase (*Fmr1*: wake $F_{(1,12)}$=117.7, P<0.0001, NREM $F_{(1,12)}$=127.8, P<0.0001, REM $F_{(1,12)}$=92.6, P=0<0.0001; BTBR: wake $F_{(1,14)}$=117.2, P<0.0001, NREM $F_{(1,14)}$=135.4, P<0.0001, REM $F_{(1,14)}$=270.5, P<0.0001). No main effects of genotype (*Fmr1:* wake $F_{(1,12)}$=1.72, P=0.21, NREM $F_{(1,12)}$=1.66, P=0.22, REM $F_{(1,12)}$=0.31, P=0.59; BTBR wake $F_{(1,14)}$=0.0004, P=0.98, NREM $F_{(1,14)}$=0.005, P=0.94, REM $F_{(1,14)}$=3.34, P=0.09) or genotype × time interactions (*Fmr1:* wake $F_{(1,12)}$=2.25, P=0.16, NREM $F_{(1,12)}$=2.65, P=0.13, REM $F_{(1,12)}$=2.03, P=0.18; BTBR wake $F_{(1,14)}$= $1 \times 10^{-0.006}$, P=0.999, NREM $F_{(1,14)}$= 0.003, P=0.96, REM $F_{(1,14)}$=0.03, P=0.86) were observed. All comparisons were made using 2-way repeated measures ANOVAs. **(D)** The number of sleep-wake transitions per hour did not differ from WT in *Fmr1* KO (NREM>wake: $F_{(1,12)}$=1.62, P=0.23; REM>wake: $F_{(1,12)}$=0.05, P=0.83) or BTBR (NREM>wake: $F_{(1,14)}$=0.21, P=0.66; REM>wake: $F_{(1,14)}$=1.71, P=0.21) mice. There was no significant genotype-time interaction for either line (*Fmr1*: NREM>wake $F_{(1,12)}$=1.96, P=0.19; REM>wake $F_{(1,12)}$=1.45, P=0.25; BTBR: NREM>wake: $F_{(1,14)}$=2.5×10^{-5}, P=0.996; REM>wake: $F_{(1,14)}$=0.001, P=0.97). There were significant main time of day effects for both lines

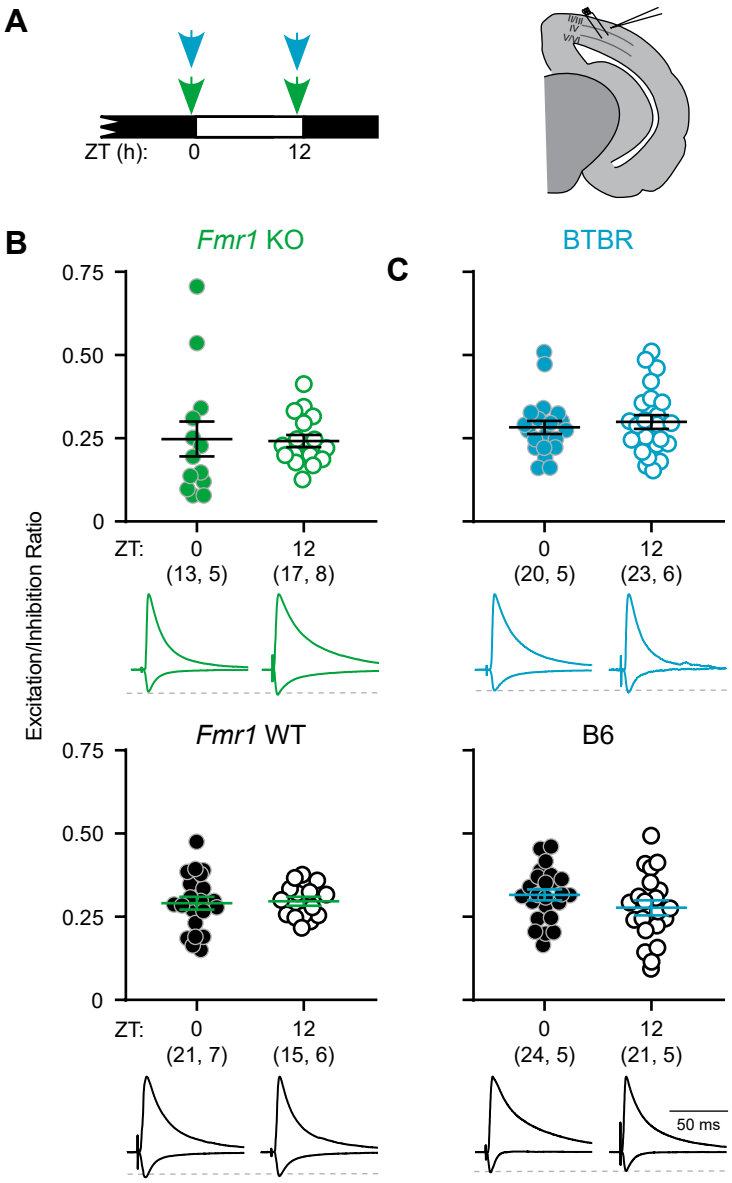
A
ZT (h):
0
12
B
Fmr1 KO
C
BTBR
Excitation/Inhibition Ratio
0.75
0.50
0.25
0
ZT:
0
12
(13, 5)
(17, 8)
(20, 5)
(23, 6)
Fmr1 WT
B6
(21, 7)
(15, 6)
(24, 5)
(21, 5)
50 ms

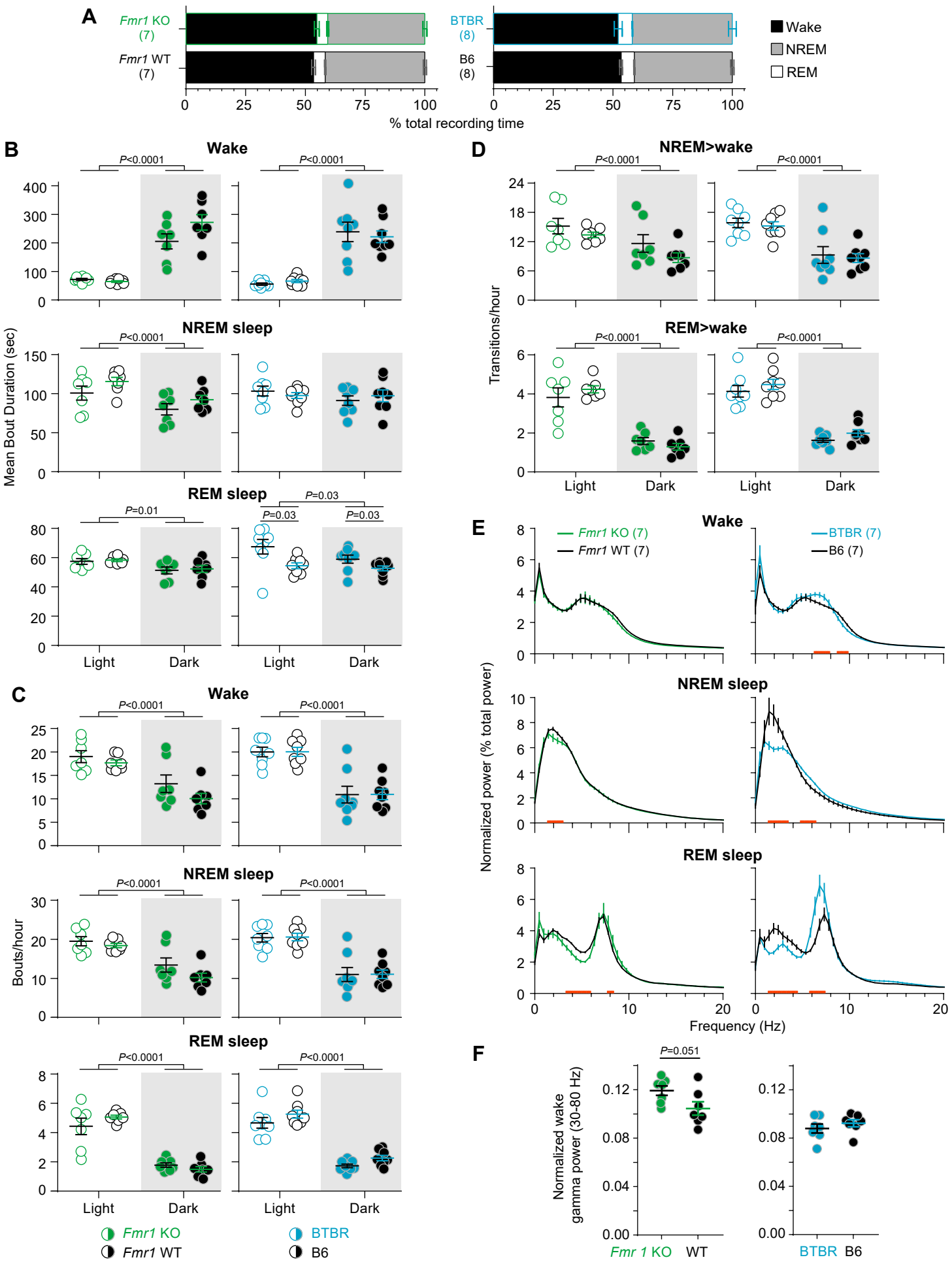
A
Fmr1 KO (7)
Fmr1 WT (7)
BTBR (8)
B6 (8)
Wake
NREM
REM
% total recording time
B
Wake
NREM sleep
REM sleep
Mean Bout Duration (sec)
P<0.0001
P=0.01
P=0.03
Light
Dark
C
Bouts/hour
D
NREM>wake
REM>wake
Transitions/hour
E
Fmr1 KO (7)
Fmr1 WT (7)
BTBR (7)
B6 (7)
Normalized power (% total power)
Frequency (Hz)
F
P=0.051
Normalized wake gamma power (30-80 Hz)
Fmr 1 KO
WT
BTBR
B6

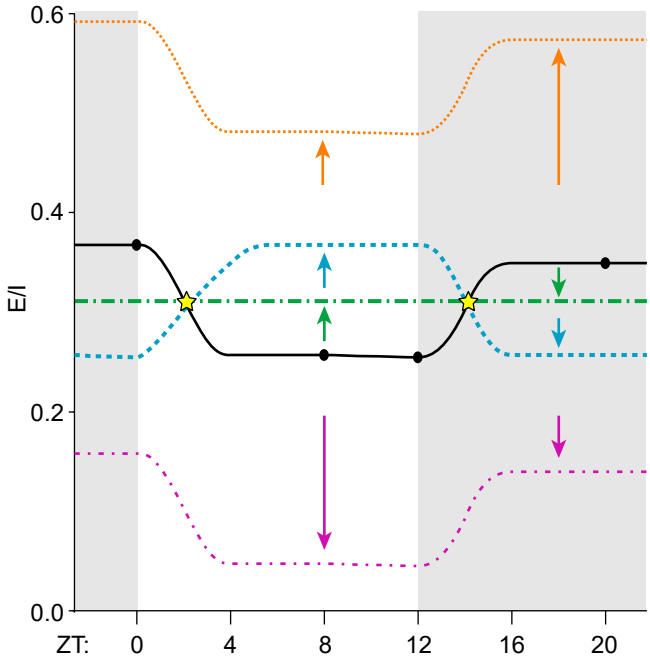
0.6
0.4
0.2
0.0
E/I
ZT:
0
4
8
12
16
20

(*Fmr1*: NREM>wake $F_{(1,12)}$=107.7, P<0.0001; REM>wake $F_{(1,12)}$=75.7, P<0.0001; BTBR: NREM>wake: $F_{(1,14)}$=57.8, P<0.0001; REM>wake: $F_{(1,14)}$=246.1, P<0.0001). **(E-F)** Power spectra were calculated separately for wake, NREM sleep, and REM sleep arousal states and normalized to total spectral power (0.5-80 Hz) within that state. **(E)** Orange lines indicate the frequencies at which genotypes are significantly different (2-way ANOVA, Holm-Sidak post-hoc test P<0.05). **(F)** Wake power in the gamma range showed a strong trend toward higher power in *Fmr1* KO than WT controls ($t_{(12)}$=2.17, P=0.051). There was no difference between B6 and BTBR mice ($t_{(12)}$=0.92, P=0.38). For all panels, sample size is indicated as (mice) and bars represent mean ± SEM.

Supplementary Figure 3. Apparent differences in the E/I ratio between WT and ASD models can arise from multiple scenarios. In WT mice, E/I ratio oscillates over the 24h day (black; circles represent mean E/I ratio at four times of day as reported in (Bridi et al., 2020)). If the E/I ratio is measured at a single time of day and is observed to be altered in a genetic mouse model, several scenarios are possible. First, the oscillation could be intact, with the E/I ratio higher (orange) or lower (purple) at all times of day. Alternatively, the oscillation could be flattened (green) or shifted in time (blue), as observed in *Fmr1* KO and BTBR mice, respectively. Both of these scenarios would result in an apparent increase or decrease in the E/I ratio, depending on the time of day it is measured. Moreover, in these scenarios, there are two times of day when the E/I ratio is equal between WT and ASD model mice (yellow stars).

SUPPLEMENTARY TABLES.

Table S1. mE/IPSC characteristics in *Fmr1* KO and WT mice. Groups were compared using *t* tests or Mann-Whitney *U* tests, as indicated. Data are shown as mean ± SEM.

		Amplitude	Frequency	Rise	Decay	N
mEPSCs	KO ZT0	13.20 ± 0.4	8.55 ± 0.6	0.79 ± 0.01	2.53 ± 0.05	38 , 5
	KO ZT12	13.67 ± 0.3	9.35 ± 0.6	0.78 ± 0.02	2.63 ± 0.06	37 , 6
	test statistic	*U*=579	*U*=613	*U*=690	*U*=592.5	
	P	0.19	0.35	0.89	0.24	
	WT ZT0	12.58 ± 0.3	8.09 ± 0.6	0.77 ± 0.02	2.60 ± 0.05	34 , 5
	WT ZT12	13.09 ± 0.4	5.27 ± 0.3	0.77 ± 0.02	2.52 ± 0.06	30 , 5
	test statistic	*U*=445	*U*=269	$t_{(62)}$=0.23	*U*=415	
	P	0.39	**0.001***	0.82	0.2	
mIPSCs	KO ZT0	46.01 ± 1.7	14.09 ± 1.0	0.65 ± 0.03	5.58 ± 0.20	39 , 6
	KO ZT12	42.60 ± 2.1	15.17 ± 1.5	0.66 ± 0.03	6.37 ± 0.28	31 , 6
	test statistic	$t_{(68)}$=1.26	*U*=596	*U*=576	$t_{(68)}$=2.36	
	P	0.21	0.93	0.74	**0.02***	
	WT ZT0	38.80 ± 2.8	11.84 ± 1.1	0.75 ± 0.05	6.00 ± 0.33	27 , 5
	WT ZT12	40.47 ± 0.2	15.83 ± 1.0	0.69 ± 0.03	5.64 ± 0.20	26 , 5
	test statistic	$t_{(51)}$=0.46	$t_{(51)}$=2.69	*U*=330.5	$t_{(51)}$=0.94	
	P	0.65	**0.0098***	0.73	0.35	

Table S2. mE/IPSC characteristics in BTBR and B6 mice. Groups were compared using *t* tests or Mann-Whitney *U* tests, as indicated. Data are shown as mean ± SEM.

		Amplitude	Frequency	Rise	Decay	N
mEPSCs	BTBR ZT0	13.6 ± 0.6	9.2 ± 0.8	0.8 ± 0.03	2.7 ± 0.1	32 , 6
	BTBR ZT12	12.8 ± 0.5	13.2 ± 1.2	0.7 ± 0.02	2.5 ± 0.1	31 , 5
	test	*t*(61)=1.08	*U*=322	*t*(61)=1.49	*t*(61)=1.60	
	P	0.28	**0.016***	0.14	0.11	
	B6 ZT0	13.7 ± 0.5	12.5 ± 1.2	0.8 ± 0.03	2.8 ± 0.1	38 , 10
	B6 ZT12	13.6 ± 0.4	8.5 ± 0.9	0.8 ± 0.03	3.1 ± 0.1	31 , 9
	test	*t*(67)=0.91	*t*(67)=2.53	*U*=511	*U*=461.5	
	P	0.11	**0.014***	0.35	0.12	
mIPSCs	BTBR ZT0	45.6 ± 2.0	24.3 ± 2.2	0.5 ± 0.01	3.8 ± 0.1	29 , 6
	BTBR ZT12	49.0 ± 3.2	17.3 ± 1.8	0.5 ± 0.02	4.0 ± 0.2	29 , 6
	test statistic	*t*(56)=0.93	*U*=278	*t*(56)=0.27	*t*(56)=0.76	
	P	0.36	**0.026***	0.79	0.45	
	B6 ZT0	45.2 ± 2.1	14.9 ± 0.9	0.5 ± 0.02	4.2 ± 0.2	36 , 6
	B6 ZT12	40.6 ± 1.8	18.6 ± 1.2	0.6 ± 0.02	4.4 ± 0.2	38 , 6
	test statistic	*t*(72)=1.71	*U*=464	*t*(72)=1.82	*U*=648	
	P	0.09	**0.017***	0.07	0.70	